Propulsion and Power Research 2014;3(1):29–40

http://ppr.buaa.edu.cn/

Propulsion and Power Research

www.sciencedirect.com

ORIGINAL ARTICLE

Compressible flow characteristics around a biconvex arc airfoil in a channel

Md. Abdul Hamid[a], A.B.M. Toufique Hasan[a,*], S.M. Alimuzzaman[a], S. Matsuo[b], T. Setoguchi[b]

[a]*Department of Mechanical Engineering, Bangladesh University of Engineering and Technology (BUET), Dhaka-1000, Bangladesh*
[b]*Department of Advanced Technology Fusion, Saga University, Saga 8408502, Japan*

Received 4 August 2013; accepted 18 November 2013
Available online 21 March 2014

KEYWORDS

Compressible flow;
Shock waves;
Shock induced oscillation;
Frequency;
Reynolds-averaged Navier-Stokes (RANS)

Abstract Shock wave-boundary layer interactions (SWBLI) are observed in several practical high-speed internal flows, such as compressor blades, turbine cascades, nozzles and so on. Shock induced oscillations (SIO), aerodynamic instabilities so-called buffet flows, flutter, aeroacoustic noise and vibration are the detrimental consequences of this unsteady shock-boundary layer interactions. In the present study, a numerical computation has been performed to investigate the compressible flow characteristics around a 12% thick biconvex circular arc airfoil in a two dimensional channel. Reynolds averaged Navier-Stokes equations with two equation k-ω shear stress transport (SST) turbulence model have been applied for the computational analysis. The flow field characteristics has been studied from pressure ratio (ratio of back pressure, p_b to inlet total pressure, p_{01}) of 0.75 to 0.65. The present computational results have been compared and validated with the available experimental data. The results showed that the internal flow field characteristics such as shock wave structure, its behavior (steady or unsteady) and the corresponding boundary layer interaction are varied with pressure ratio. Self-excited shock oscillation was observed at certain flow conditions.

*Corresponding author: Tel.: +880 1730714444.
E-mail address: toufiquehasan@me.buet.ac.bd (A.B.M. Toufique Hasan).

Peer review under responsibility of National Laboratory for Aeronautics and Astronautics, China.

Production and hosting by Elsevier

http://dx.doi.org/10.1016/j.jppr.2014.01.002

Moreover, the mode of unsteady shock oscillation and its frequency are varied significantly with change of pressure ratio.

1. Introduction

Shock wave-boundary layer interactions (SWBLI) are not only fundamental research topics of aerodynamics but are observed in several practical high-speed internal flows, such as turbine cascades, compressor blades, butterfly valves, fans, nozzles, diffusers and so on. Shock induced oscillations (SIO), aerodynamic instabilities so-called buffet flows, high cycle fatigue failure (HCF), nonsynchronous vibration (NSV), flutter, aeroacoustic noise and vibration and so on are the detrimental consequences of unsteady shock/boundary layer interactions [1–3]. McDevitt et al. [4] and Levy [5] performed an experimental and theoretical study of transonic flow over a 18% thick arc airfoil. The results stated that the shock-boundary layer interaction phenomena are strongly dependent on Mach number and Reynolds number. Tijdeman [6] had described the behavior of the transonic flow around an oscillating airfoil. The interaction of steady and unsteady flow fields and periodic motion of the shock were focused in that study. Yamamoto and Tanida [7] investigated the self-excited oscillation of transonic flow in a cascade model. The measurements of the shock wave and wake motions, and the unsteady static pressure field predicted a closed loop mechanism for the self-excited shock oscillation. In the same year, Lee [8] proposed and quantified a feed-back mechanism of shock oscillation for flow over a supercritical airfoil. It was observed that the time to take a disturbance to propagate from the shock to the trailing edge plus the additional time it takes for an upstream traveling wave generated at the trailing edge to reach the shock agreed quite closely with the period of shock oscillation measured from unsteady force spectra. Alshabu et al. [9] investigated the upstream moving pressure wave for shock oscillation around a supercritical airfoil. Time-resolved pressure measurements revealed the unsteady behavior of these waves and the measured frequencies were in the order of kHz. Raghunathan et al. [10] performed a computation using thin-layer Navier-Stokes approximate to investigated the origin of shock oscillation around a 18% thick biconvex aerofoil. Results indicated that the shock induced separation plays the leading role of the origin of shock oscillation. However, in the review article of Lee [11], it was concluded that the complete understanding of the mechanisms responsible for self-sustained oscillations of the shock waves under wide ranges of conditions, such as Mach number, incidence angle, Reynolds number, and airfoil geometry has not yet been achieved.

Recently, Xiong et al. [12] performed a 2D numerical simulation using Unsteady Reynolds Averaged Navier-Stokes (URANS) and Detached Eddy Simulation (DES) to investigate the transonic shock oscillation over a 10% thick circular arc airfoil in a channel. These methods could predict the overall shock oscillatory behavior. However, the computationally obtained frequency varied considerably in the range of 50% to 100% with the experimental frequency of Yamamoto and Tanida [7]. Chen et al. [13] performed a DES study of compressible flow past a 18% thick circular arc airfoil. Various fundamental mechanisms dictating the intricate flow phenomena such as moving shock wave behaviors, turbulent boundary layer characteristics, kinematics of coherent structures had been studied. Moreover, the effect of air humidity on the shock oscillation around an airfoil in 2D channel was performed by Hasan et al. [14]. And it was revealed that the non-equilibrium condensation of moist air reduces the unsteady shock behavior compared to dry air case.

Though there have been a great deal of researches on high speed aerodynamics over airfoils, the understanding of the compressible flow characteristic over an airfoil in a channel is not completely clear until now. In the present study, a 2D numerical computation is performed to investigate the shock wave generation and its behavior in compressible flows around a 12% thick biconvex circular arc airfoil. Different compressible flow conditions are considered by varying the pressure ratio, *PR* which is defined as the ratio of back pressure to inlet total pressure. The steady shock wave and shock waves with unsteady oscillation in the flow field are captured at different flow conditions. Various aerodynamic parameters such as time histories of static pressure, root mean square (RMS) of pressure oscillation and fundamental frequency of shock oscillation are discussed.

2. Numerical methods

2.1. Governing equations

The flow field in this study is considered to be viscous, compressible, turbulent, and unsteady. Governing equations for the present RANS computations are the conservation of mass, conservation of momentum and the energy equations written in 2D coordinate system (x, y). Two additional transport equations of k-ω SST (Shear Stress Transport) turbulence model [15] are included to model the turbulence in the flow field. The governing equation can be written in the following vector form:

$$\frac{\partial \boldsymbol{U}}{\partial t}+\frac{\partial \boldsymbol{E}}{\partial x}+\frac{\partial \boldsymbol{F}}{\partial y}=\frac{\partial \boldsymbol{R}}{\partial x}+\frac{\partial \boldsymbol{S}}{\partial y}+\boldsymbol{H} \tag{1}$$

Nomenclature

c	chord length of the airfoil (unit: mm)
$\boldsymbol{E}$	inviscid flux vector in x-direction
$\boldsymbol{F}$	inviscid flux vector in y-direction
f	frequency of shock oscillation (unit: Hz)
H	height of the channel (unit: mm)
$\boldsymbol{H}$	turbulence source term
Ma	Mach number
n	number of sampling points
p	static pressure (unit: kPa)
PR	pressure ratio
q	dynamic pressure (unit: kPa)
Re	Reynolds number
$\boldsymbol{R}$	viscous flux vector in x-direction
R	circular arc radius (unit: mm)
RMS	root mean square
$\boldsymbol{S}$	viscous flux vector in y-direction
$\boldsymbol{U}$	conservative flux vector
x	streamwise coordinate (unit: mm)
y	normal coordinate (unit: mm)
T	time period (unit: s)
t	time (unit: s)/thickness (unit: mm)

Subscripts

b	back pressure
i	instantaneous state
0	upstream condition
0l	total/stagnation condition at inlet
s	shock wave

Here $\boldsymbol{U}$ is the conservative flux vector. $\boldsymbol{E}$ and $\boldsymbol{F}$ are the inviscid flux vectors and $\boldsymbol{R}$ and $\boldsymbol{S}$ are the viscous flux vectors in the x and y directions, respectively. $\boldsymbol{H}$ is the source terms corresponding to turbulence.

The governing equations are discretized spatially using a Finite volume method of second order scheme. For the time derivatives, an implicit multistage time stepping scheme, which is advanced from time t to time $t+\Delta t$ with a second order Euler backward scheme for physical time and implicit pseudo-time marching scheme for inner iteration, is used. A time step size of 10^{-7} was found sufficient for this type of unsteady computation. The viscosity is considered to vary according to Sutherland's law.

2.2. *Computational domain and boundary conditions*

Figure 1(a) shows the computational domain with boundary conditions for the present problem. Close view of arc airfoil with grids is shown in Figure 1(b).

Chord length, c of the circular arc airfoil is 48 mm. The leading and trailing edges of the airfoil are kept sharp. The thickness, t and the radius of the circular arc, R are $0.12c$ and $1.7c$, respectively. Computational domain is discretized by structured mesh with 60,482 grids which gives grid independent solution. The typical distribution of wall $y+$ along the airfoil upper and lower surfaces is shown in Figure 1(c). The minimum normal grid spacing was reduced to $8.3 \times 10^{-5}c$ (≈ 4 μm) which gives the value of $y+ \approx 0.4$ near the solid surface. This wall grid spacing can be considered enough to capture the boundary layer separation by the unsteady shock waves. The origin of (x, y) coordinate is located at leading edge of the airfoil. The pressure ratio, $PR = p_b/p_{01}$, where p_b is outlet pressure and p_{01} is the inlet total pressure, was varied from 0.75 to 0.65 successively with an interval of 0.01. The inlet Mach number upstream of the airfoil was 0.60. The corresponding Reynolds numbers based on the airfoil chord is 5×10^5. The angle of attack was kept constant at 0°. At the inlet, stagnation (total) pressure and temperature were imposed as physical boundary conditions and the other variables were resulted from the numerical boundary treatment through Riemann invariant.

The exit boundary was constrained with pressure outlet boundary condition. The inlet total pressure was kept constant at 101,325 Pa and outlet pressure is continuously decreased to generate different flow cases. Non-slip and adiabatic wall conditions were applied at the solid boundary. The pressure at the wall was obtained from zero normal pressure gradients on the body surface.

3. Computational validation

Before going to the detail discussion, the present numerical methods will be validated with the available experimental results. Since the experimental flow structures are available for 15% thick arc airfoil [14], the present simulation was first carried out with the same airfoil for verification of numerical schemes. Figure 2(a) shows the Schlieren image obtained from the experiments of Hasan et al. [14] for $p_{b0}/p_{01} = 0.70$. The same flow case corresponds to $p_b/p_{01} = 0.69$ which is defined as the pressure ratio, PR in the present study. The numerically obtained flow field with shock waves is shown in Figure 2(b). It is found that the flow structures are almost similar to the experimental results except the locations of shock waves. For further verification, distribution of time-average pressure coefficient is shown in Figure 3. The solid line represents the present computational results and open circle symbol represents experimental results of McDevitt et al. [4]. The computational results slightly over predict the value of c_p in the mean shock position and the region of the intense shock boundary layer interaction. The differences in shock structure and pressure coefficient are obviously due to the complexities in real flows, the mean flow non-uniformity and the sidewall boundary layer, which are never taken into account in present 2D numerical computation.

In addition to the above discussion, the unsteady shock oscillation frequencies are taken into consideration for further validation. Figure 4 shows the oscillation frequency for the case of 12% thick airfoil. The open circle symbol is for experimental results of Yamamoto and Tanida [7] (turbulent boundary layer case) while the closed circle symbol is for results from present computation. Both results shows the same variation of frequency with *PR*. However, the present 2D computation predicts oscillation frequencies which are 25% to 40% higher in magnitude compared to experimental ones. This means that there might be three dimensional mechanisms that govern the oscillation frequency. Similar observations were mentioned in the work of Xiong et al. [12].

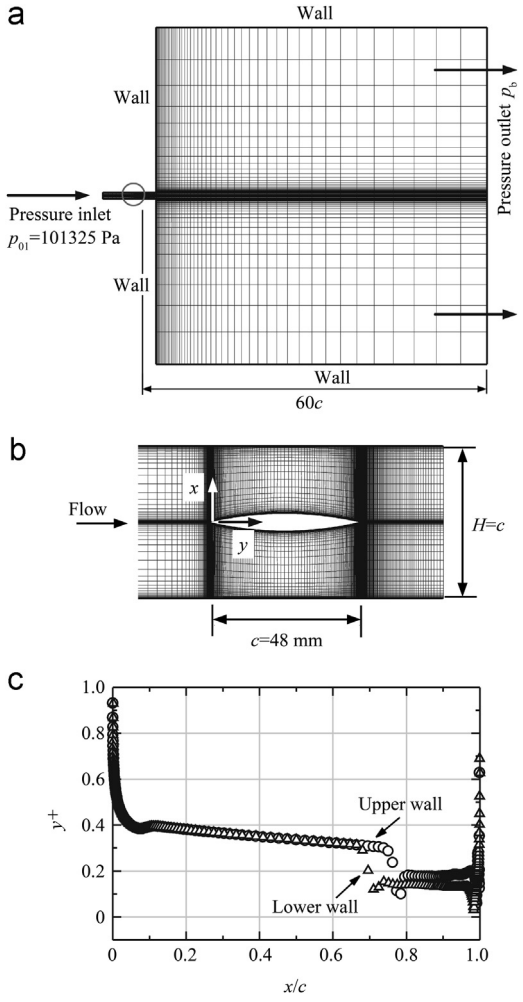

Figure 1 (a) Computational domain with boundary conditions, (b) close view of arc airfoil with grids and (c) distribution of near wall *y*+.

4. Results and discussion

While varing the pressure ratio, *PR* transition between steady and unsteady flow behavior has been noticed. For higher pressure ratio (*PR* greater than 0.73), the flow field is steady and subsonic throughout the entire region. For pressure ratio, *PR* of 0.73 and 0.72, a local supersonic

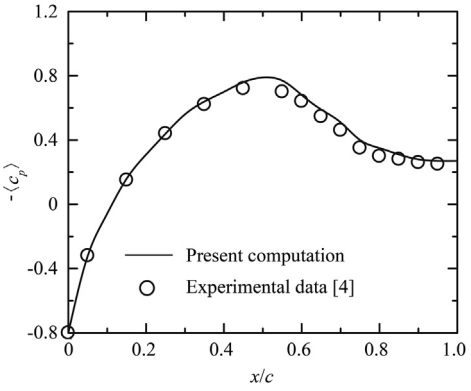

Figure 3 Distribution of time averaged pressure coefficient.

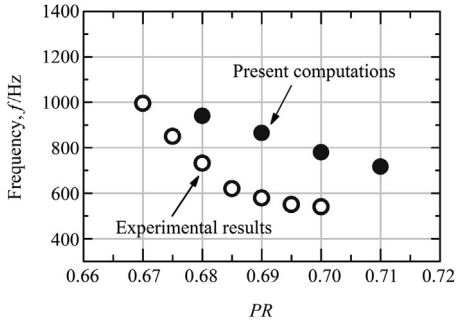

Figure 4 Relation between shock wave frequency and pressure ratio (12% thick airfoil).

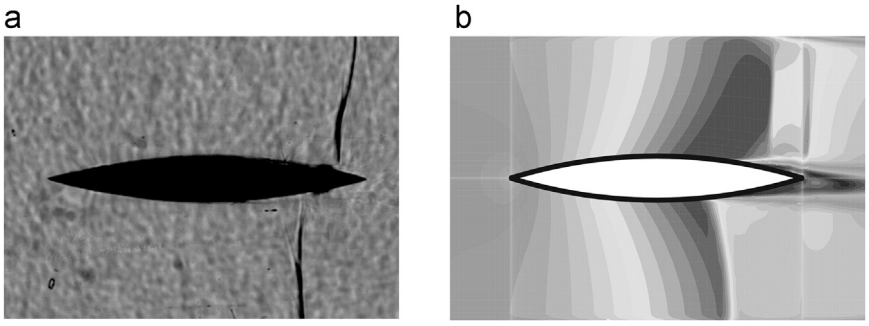

Figure 2 Instantaneous flow field with shock waves. (a) Experimental Schlieren photograph [14] for $p_{b0}/p_{01}=0.70$ and (b) Mach contour from present computation for $p_b/p_{01}=0.69$ (15% thick airfoil).

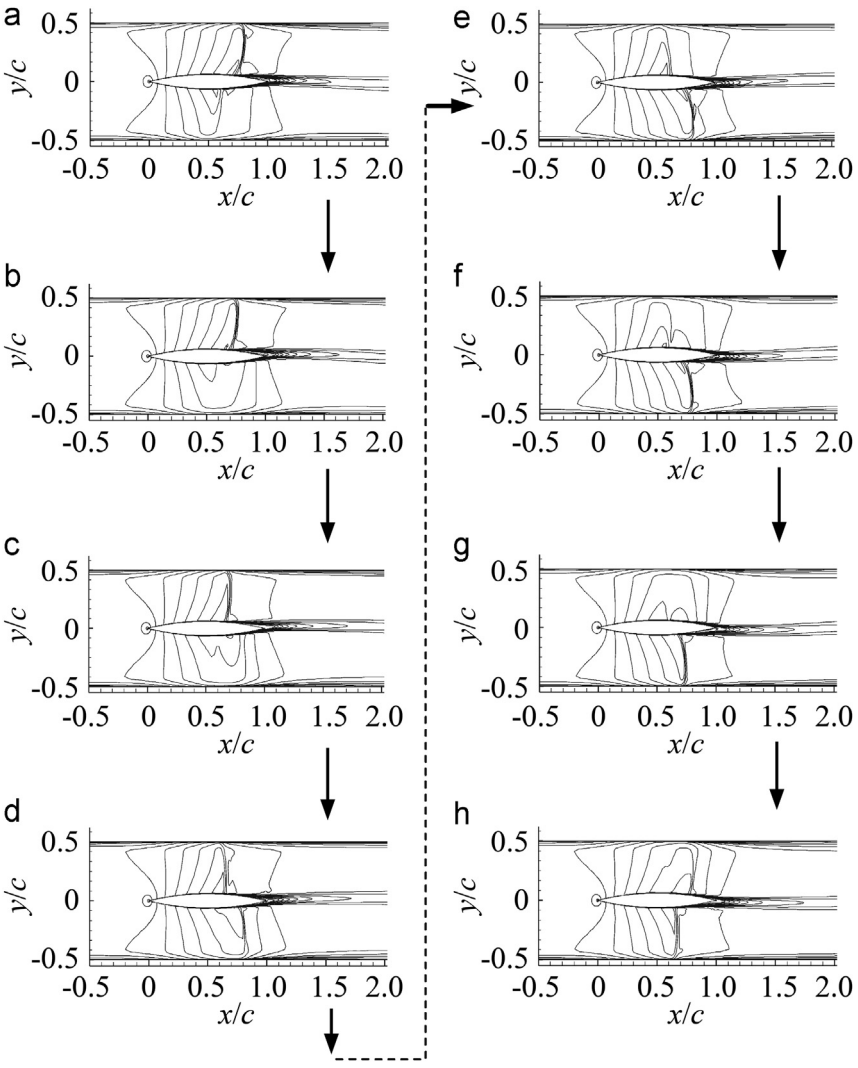

Figure 5 Sequential contour maps of Mach number during one cycle of shock oscillation for $p_b/p_{01}=0.71$. (a) $t/T=0$, (b) $t/T=1/8$, (c) $t/T=2/8$, (d) $t/T=3/8$, (e) $t/T=4/8$, (f) $t/T=5/8$, (g) $t/T=6/8$ and (h) $t/T=7/8$.

bubble is formed and the shock waves are weak in strength with shock Mach number, Ma_s of 1.06 and 1.16, respectively. For pressure ratio of 0.71 to 0.68, the flow becomes unsteady. Figure 5 shows the sequential contour maps of Mach number during one cycle of flow oscillation for $p_b/p_{01}=0.71$. To investigate the unsteady shock behavior, the time period of shock oscillation, T is sub-divided into eight equal steps. T is calculated at the position of peak RMS of pressure oscillation (will be discussed latter). At this case, normal shock waves are observed around the upper and lower surfaces of the airfoil. At the beginning of the oscillation, $t/T=0$ (Figure 5(a)), the shock appeared along the upper surface only at $x/c=0.72$. Compression wave is seen along the lower surface at $x/c=0.55$ at this time. At $t/T=1/8$ (Figure 5(b)), the upper shock moves slightly upstream to $x/c=0.70$ and the lower shock is disappeared. At $t/T=2/8$ (Figure 5(c)), the upper shock moves further upstream to $x/c=0.64$ and the lower shock is started to generate from $x/c=0.72$. Next the upper shock moves to $x/c=0.60$ and its strength reduces at $t/T=3/8$ (Figure 5(d)). At this time, the wave at lower surface gets stronger. In the next half cycle, the upper shock moves further upstream with reduced strength, becomes compression wave and finally disappear at $t/T=7/8$ as shown in Figure 5(g). However, the lower shock gets stronger compared to upper wave in these instants. Thus the normal shock oscillates alternatively in between upper and lower surfaces at this flow case. By decreasing the PR to 0.70 and 0.69, the similar flow behaviors are observed and flow fields are not shown here for brevity.

For $p_b/p_{01}=0.68$, a different flow structure is observed and the sequential contour maps of Mach number during one cycle of shock oscillation are shown in Figure 6. In this case λ-shock wave appeared in the channel passage. Shock waves are always present around the upper and lower surfaces of the airfoil during the cycle. At $t/T=0$ (Figure 6(a)), the λ-shock waves are observed at $x/c=0.76$ and 0.68 for upper and lower surfaces, respectively. Then the upper shock wave moves upstream to $x/c=0.72$ and the lower surface shock wave moves downstream to $x/c=0.72$

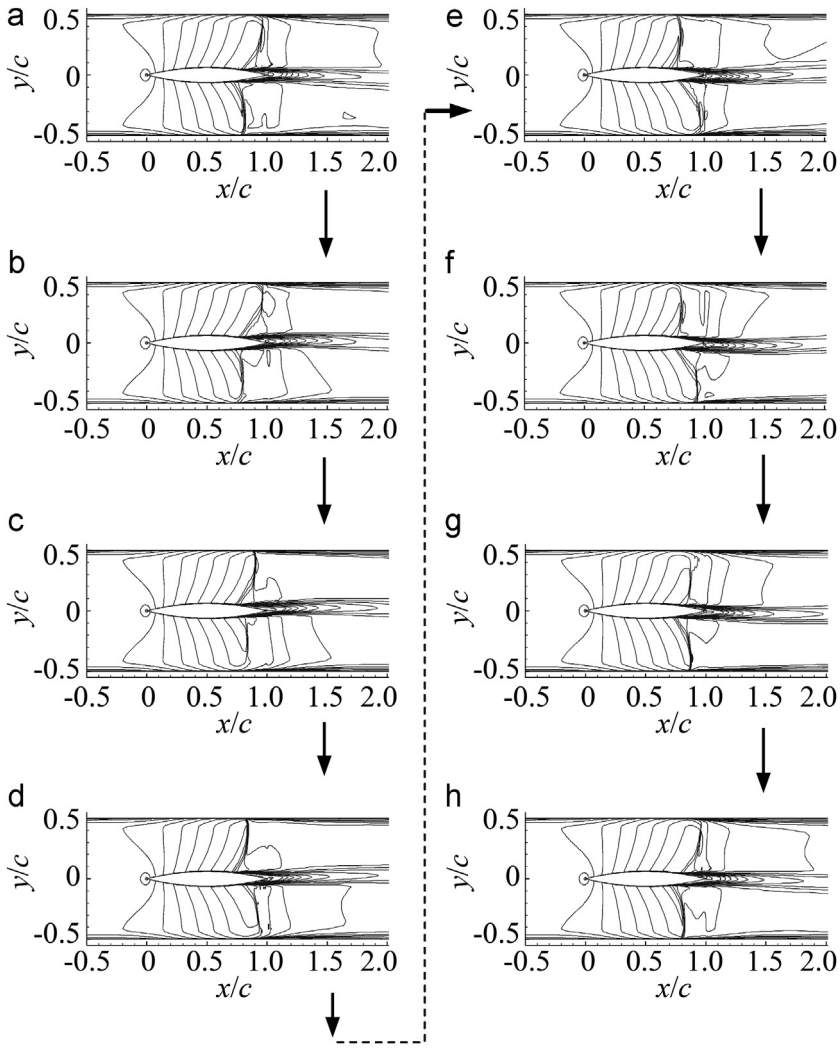

Figure 6 Sequential contour maps of Mach number during one cycle of shock oscillation for $p_b/p_{01}=0.68$. (a) $t/T=0$, (b) $t/T=1/8$, (c) $t/T=2/8$, (d) $t/T=3/8$, (e) $t/T=4/8$, (f) $t/T=5/8$, (g) $t/T=6/8$ and (h) $t/T=7/8$.

at $t/T=1/8$ as shown in Figure 6(b). At next instant, $t/T=2/8$ (Figure 6(c)), the upper surface shock moves further upstream to $x/c=0.68$ and the lower shock moves further downstream to $x/c=0.76$. Both shock waves change their shapes but remain at the same positions at $t/T=3/8$ (Figure 6(d)). Thus completes the half cycle of shock oscillation. In the next half cycle, the upper surface and lower surface shock waves move downstream and upstream, respectively. The shock movements are shown successively in Figure 6(e–g). At the end of cycle, $t/T=7/8$ (Figure 6(h)), the upper and lower shock waves reached their extreme positions of $x/c=0.76$ and 0.68, respectively. Thus, the λ-shock waves oscillates alternately in between upper and lower surfaces at this flow case.

The unsteady shock waves strongly interact with the boundary layers and generate the flow instability around the airfoil. Figure 7 shows the streamline pattern around the airfoil trailing edge during one cycle for $p_b/p_{01}=0.68$. Pressure contour is also shown in the figure for reference. It is found that boundary layer sepration occurs due to the interaction of shock waves and the separation behavior is unsteady in nature. Massive separation bubbles are found around the airfoil upper surface at $t/T=2/8$ (Figure 7(c)). At this time, boundary layer only separates from the lower surface and there is no formation of separation bubble. After that, the size of the separation bubble decreases along the upper surface at $t/T=3/8$ (Figure 7(d)). Along the lower surface, separation characterics intensified in the successive times and the separation bubble grows in biggest size at $t/T=5/8$ as shown in Figure 7(f).

The mechanism of unsteady self-excited shock oscillation can be described with the help of Lee's model [8,12]. Lee proposed that in case of unsteady shock movement around airfoil, pressure waves are formed which propagate downstream in the separated region. On reaching the trailing edge, the disturbances generate upstream moving waves either from the wake fluctuation or from the trailing edge boundary layer.

These waves will interact with the shock wave and impart energy to maintain its oscillation. The loop is then

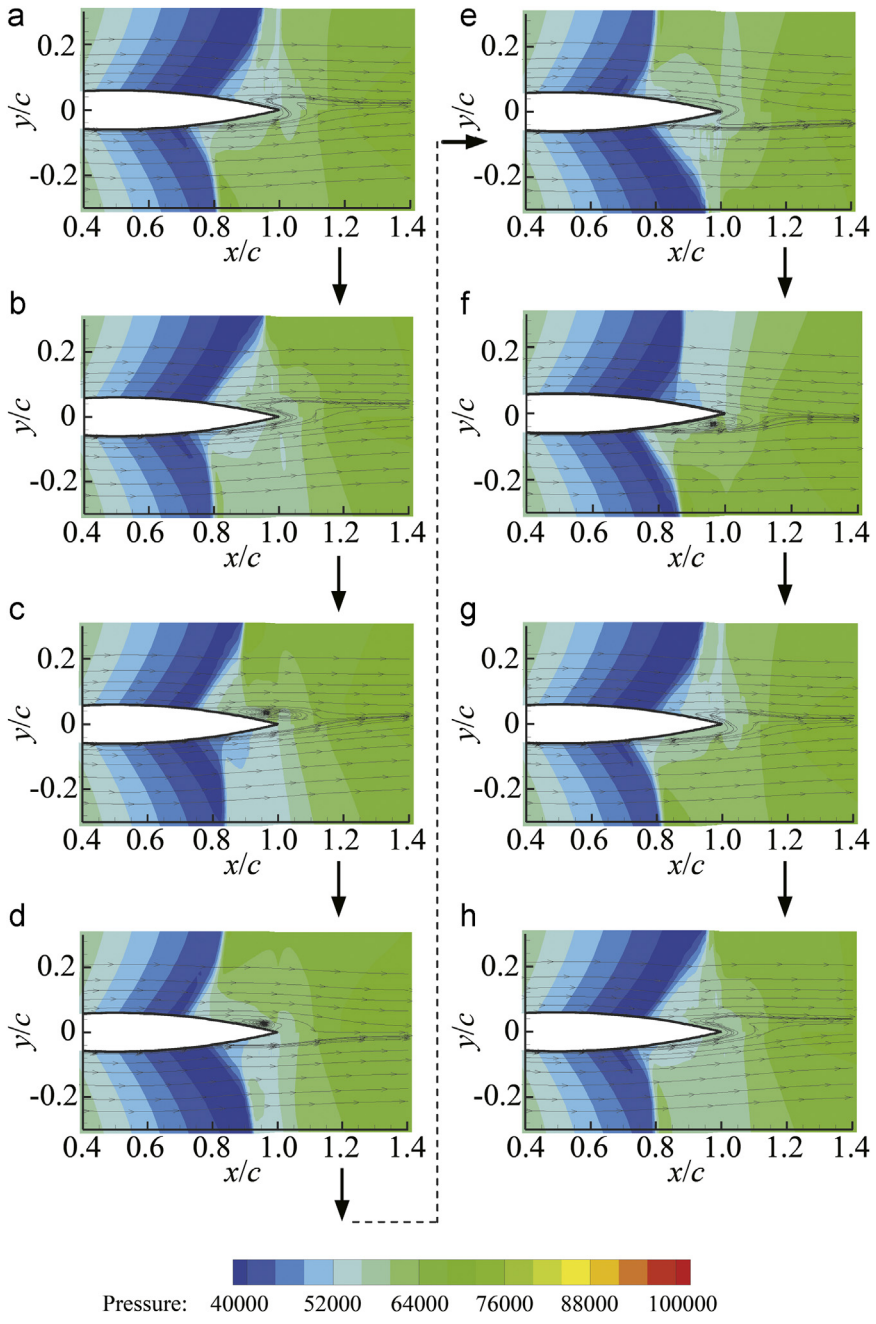

Figure 7 Streamline around the airfoil trailing edge for $p_b/p_{01}=0.68$. (a) $t/T=0$, (b) $t/T=1/8$, (c) $t/T=2/8$, (d) $t/T=3/8$, (e) $t/T=4/8$, (f) $t/T=5/8$, (g) $t/T=6/8$ and (h) $t/T=7/8$.

completed. Figure 7 presents the separation is unsteady in nature and alternates in between upper and lower surfaces around the present biconvex airfoil. Moreover, the wake fluctuations can be seen from these figures. These separation and wake fluctuation generates the downstream and upstream pressure waves alternatively. Though these waves are not calculated in detail in the present study, it can be considered that these waves play the main role to maintain the self-excited unsteady shock oscillation according to the Lee's model.

The unsteady shock oscillation generates the fluctuating Mach number just ahead of the shock wave, Ma_s. Results during one cycle of shock oscillation is shown in Figure 8 for the cases of unsteady flows. Ma_s varies periodically during the cycle. The shock Mach number varies from 1.18–1.24, 1.20–1.28, 1.25–1.31 and 1.28-1.32 for $PR=0.71$, 0.70, 0.69, and 0.68, respectively. Moreover, the Ma_s increases with decrease in PR which means that the flow expands more in the lower PR region.

Time histories of streamwise shock location, x_s/c along upper and lower surfaces are shown in Figure 9 for the unsteady flow cases of $PR=0.71$ to 0.68. The solid line with circles and cross represent the shock position on upper and lower surfaces, respectively. However, the dashed line

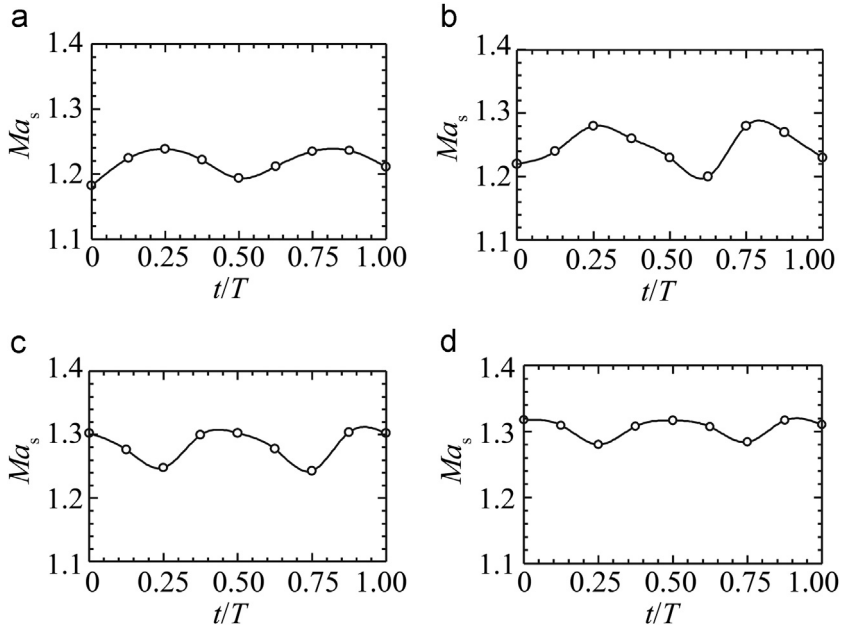

Figure 8 Time histories of shock Mach number. (a) $p_b/p_{01}=0.71$, (b) $p_b/p_{01}=0.70$, (c) $p_b/p_{01}=0.69$ and (d) $p_b/p_{01}=0.68$.

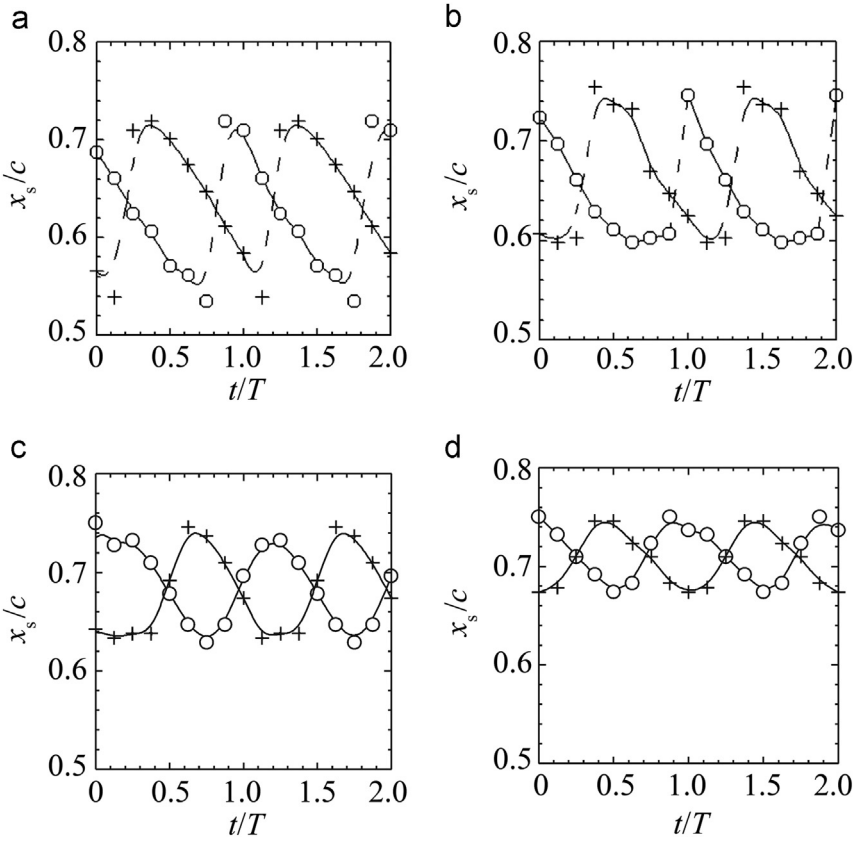

Figure 9 Time histories of shock position, x_s. (a) $p_b/p_{01}=0.71$, (b) $p_b/p_{01}=0.70$, (c) $p_b/p_{01}=0.69$ and (d) $p_b/p_{01}=0.68$.

is for no shock wave. For all the cases, periodic shock oscillations are observed. For higher pressure ratio, *PR* of 0.71 (Figure 9(a)) and 0.70 (Figure 9(b)), though the shock is moving but the movement is discontinuous. At the instances when there is a shock on upper surface, lower surface remains with no shock and vice versa. This shock oscillation is known as Tijdeman type B [6]. The length of shock excursion zone is $0.17c$ with mean shock position, $(x_s)_{mean}$ is at $0.62c$ for $PR=0.71$. At $PR=0.70$, shock oscillates within $0.12c$ and the $(x_s)_{mean}$ is at $0.66c$. For

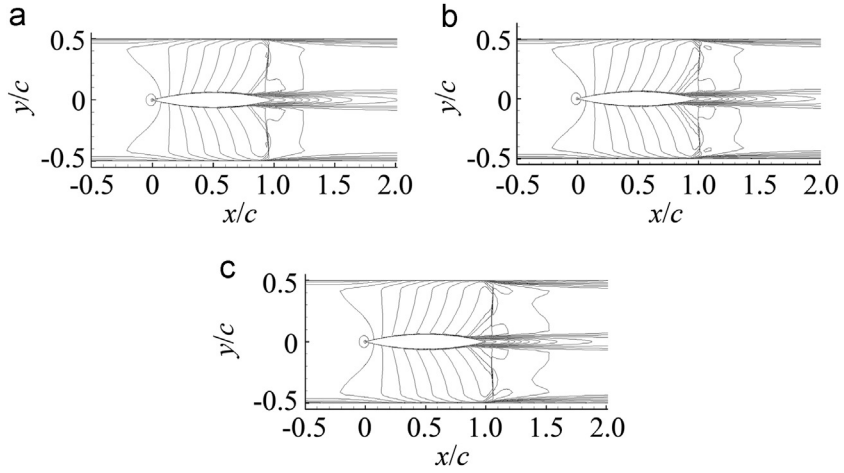

Figure 10 Contour maps of Mach number for (a) $p_b/p_{01}=0.67$, (b) $p_b/p_{01}=0.66$ and (c) $p_b/p_{01}=0.65$.

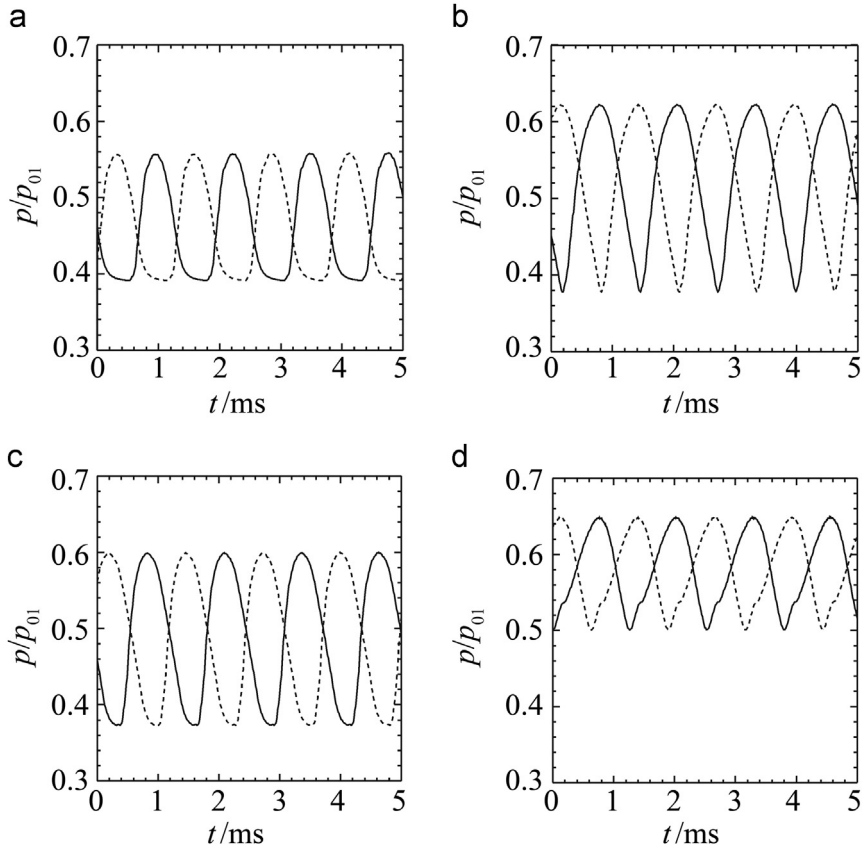

Figure 11 Time histories of static pressure at $p_b/p_{01}=0.71$. (a) $x/c=0.67$, (b) $x/c=0.71$, (c) $x/c=0.75$ and (d) $x/c=0.83$.

lower pressure ratio of $PR=0.69$ (Figure 9(c)) and 0.68 (Figure 9(d)), the shock movement is continuous. In these cases, the upper surface shock wave moves upstream towards the leading edge while the lower surface shock wave moves downstream towards the airfoil trailing edge. However, the channel passage remains with shock waves all through the flow oscillation period. This shock oscillation is Tijdeman type A [6]. Streamwise lengths of shock excursion zones are $0.10c$ and $0.08c$ for $PR=0.69$ and 0.68, respectively. The corresponding mean shock locations are at $0.69c$ and $0.72c$.

The flow field becomes steady for PR less than 0.68. Contour maps of Mach number for $PR=0.67$, 0.66 and 0.65 are shown in Figure 10(a–c), respectively. In these cases, the foots of the λ-shocks are clearly visible both along the upper and lower surfaces of the airfoil. The flow fields become more expanded compared to $PR=0.68$ (Figure 6). The Mach number just upstream of the shock

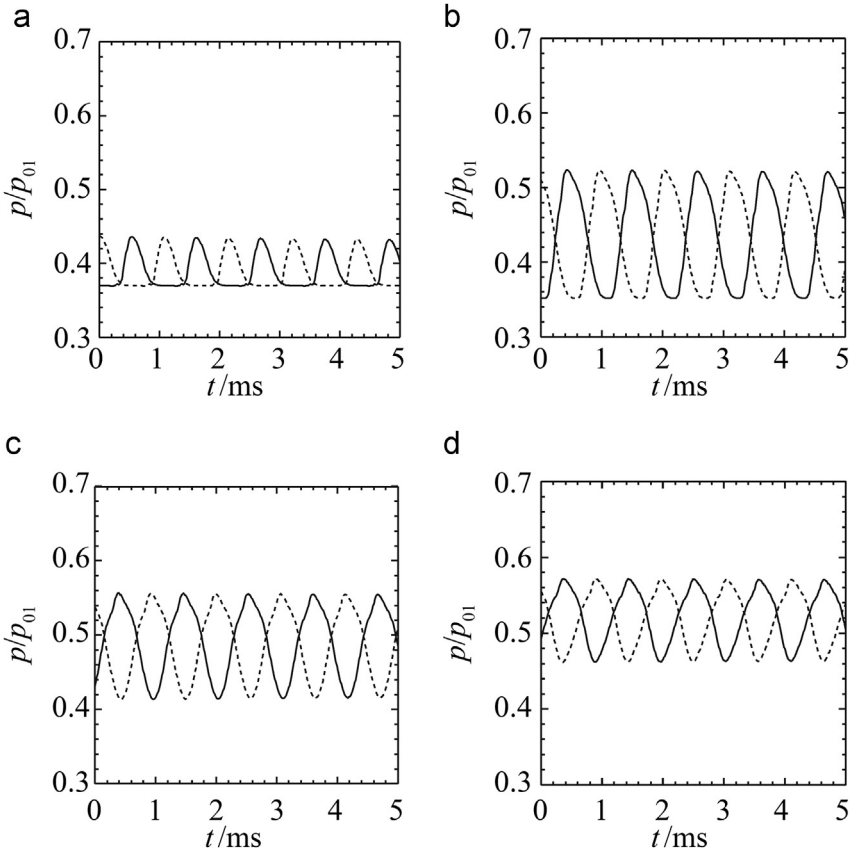

Figure 12 Time histories of static pressure at $p_b/p_{01}=0.68$. (a) $x/c=0.67$, (b) $x/c=0.77$, (c) $x/c=0.80$ and (d) $x/c=0.83$.

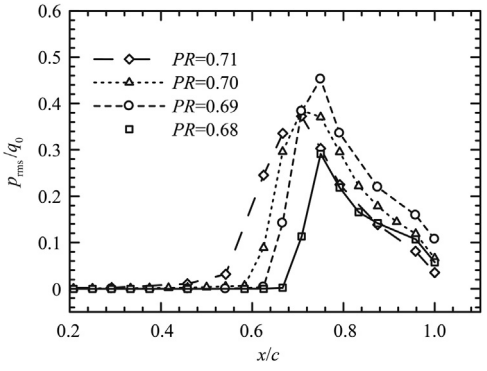

Figure 13 RMS of pressure fluctuations for different *PR*.

is increased and the λ-shock becomes stronger successively with decrease in *PR*. However, λ-shocks are not moving with time in these cases. The flow field downstream of the airfoil trailing edge are more affected with decrease in *PR*.

The time histories of static pressure at different streamwise locations for $PR=0.71$ are shown in Figure 11. The presented solid and dotted lines are for upper and lower surfaces, respectively. The static pressure fluctuation (which is produced by the unsteady shock oscillation) increases in downstream location and reaches the maximum amplitude of $\Delta p/p_{01}=0.24$ at $x/c=0.71$ as shown in Figure 11(b). After the intense shock-boundary layer interaction, the amplitude decreases further downstream locations for example at $x/c=0.83$ (Figure 11(d)). Moreover, it is confirmed that the upper and lower surfaces shock waves are 180° out of phase corresponding to shock structures as shown in Figure 5.

Results of static pressure-time histories for $PR=0.68$ are shown in Figure 12. In this case the maximum amplitude of $\Delta p/p_{01}$ is 0.16 and the location is at $x/c=0.77$ as shown in Figure 12(b). After this point, the amplitude of unsteady shock oscillation reduces successively in downstream locations. However, the pressure-time history also confirmed the alternate shock oscillation (180° out of phase) in between upper and lower airfoil surfaces as described in Figure 6.

The flow field aerodynamic instability around the circular arc airfoil can conveniently be explained by the distribution of root mean square (RMS) value of pressure oscillation induced by shock oscillation. The RMS of pressure oscillation, p_{rms} is calculated as

$$p_{rms}=\sqrt{\sum_{i=1}^{n}(p_i-\overline{p})^2/n} \quad \text{where} \quad \overline{p}=\sum_{i=1}^{n}p_i/n \tag{2}$$

In the above equation, p_i and $\overline{p}$ are the instantaneous and mean static pressures, respectively. Results are calculated for the number of sampling points, $n=10^5$ from 30 cycles. Figure 10 shows the distribution of RMS value of pressure oscillation p_{rms}/q_0 (p_{rms}: RMS of pressure oscillation; q_0: dynamic pressure upstream of the airfoil) around upper

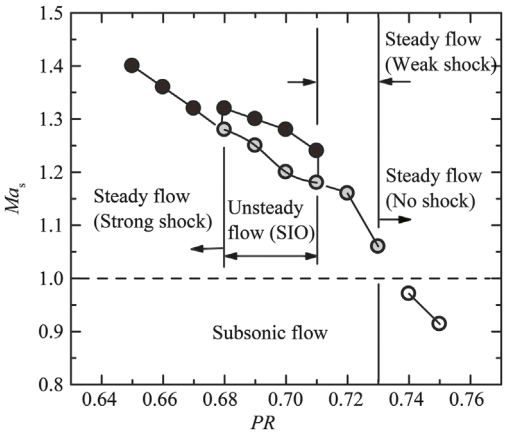

Figure 14 Flow field classification for compressible flow around a 12% thich biconvex arc airfoil in a channel at zero angle of attack.

passage of the airfoil. Figure 13 shows the distribution of RMS values of pressure oscillation at different *PR*. It is found that, for all the *PR* cases, the flow field remains steady or undisturbed up to certain position of the airfoil. The positions where the RMS values start to increase are $x/c=0.54$, 0.58, 0.64, and 0.68 for $PR=0.71$, 0.70, 0.69, and 0.68, respectively. After these positions, the RMS values increase gradually, reach the peak and then decrease. The peak RMS values are $0.37q_0$, $0.39q_0$, $0.45q_0$ and $0.30q_0$ for $PR=0.71$, 0.70, 0.69, and 0.68, respectively. The reduction of RMS values for lower pressure ratio, $PR=0.68$ is due to the formation of λ-shock wave (with reduced strength along the airfoil surface) instead of normal shocks in other unsteady cases. Moreover, the positions where peak RMS value are observed are $x/c=0.71$, 0.72, 0.75 and 0.75 for $PR=0.71$, 0.70, 0.69, and 0.68, respectively.

To determine the fundamental frequency of shock oscillation at the position of peak RMS value (Figure 13), the FFT is performed and the results have already been shown in Figure 4. The shock oscillation frequencies are 717 Hz, 780 Hz, 865 Hz, and 940 Hz for $PR=0.71$, 0.70, 0.69, and 0.68, respectively.

Finally, the compressible flow fields characteristics for internal flow around a 12% thick circular arc airfoil at zero incidence are shown in Figure 14. The shock Mach number, Ma_s is plotted againt different pressure ratio, *PR*. From the detail computational results, the flow fields can be classified into four groups as follows: Case-I (for *PR* higher than 0.73) - where there is no shock waves appeared in the flow fields; Case-II (for $PR=0.73$ to 0.71) - the flow fields with weak shocks or compression waves (localized supersonic bubble/s) and steady. Case-III ($PR=0.71$ to 0.68) - the flow fields are unsteady. In this case, shock waves are moving in continuous or discontinuous manner depending on *PR*. And the corresponding shapes of the shock waves can be normal or λ-type. The intensity of shock wave-boundary layer interactions (SWBLI) periodically varies during the oscillation. A loop of Ma_s (with lowest and highest Ma_s values) corresponds to the unsteady shock oscillation can be seen in the figure. Further, Case-IV (*PR* lower than 0.68) - where the flow becomes steady again with λ-shaped shock waves both along the upper and lower surfaces. The flow fields downstream the airfoil trailing edge is mostly affected in this case.

5. Conclusions

In the present study, a numerical computation is carried out to investigate the compressible flow field characteristics around a biconvex circular arc airfoil in a two-dimensional channel. The Mach number upstream of the airfoil is kept at 0.60 with zero angle of attack. The pressure ratio, *PR* is varied from 0.75 to 0.65. The computational results are validated with available experimental data. The results of the present study can be summarized as below:

- The flow fields remain steady with weak shock waves/ compression waves at $PR=0.73$ to 0.71.
- The self-excited shock oscillation is observed around the airfoil in the range of *PR* of 0.71 to 0.68. Unsteady shock oscillations with normal shocks and λ-shocks are found for $PR=0.71$ to 0.69 and $PR=0.68$, respectively.
- The unsteady shock movement creates the transient shock-boundary layer interaction and thus generates the unsteady separation. This unsteady separation is responsible for the self-excited shock oscillation.
- The shock Mach number and the positions of shock waves follow the periodic behavior corresponding to unsteady shock oscillation.
- The flow field becomes more unstable (with higher RMS values of static pressure fluctuations) for lower pressure up to $PR=0.69$. At $PR=0.68$, the peak RMS value of pressure oscillation reduces compared to other unsteady cases.
- The fundamental frequency of shock oscillation increases with decrease in pressure ratio.
- In cases of pressure ratio less than 0.68, the flow fields become steady again with λ-shock waves both along the upper and lower airfoil surfaces.

The findings of the present research can be used for further clarification of the characteristics of unsteady transonic shock oscillation around an airfoil for internal flow applications. Next attempt should be paid to suppress the shock induced flow unsteadiness for the safe and reliable operation of high-speed turbomachines.

Acknowledgement

The present work has been carried out with computational resource support from Higher Education Quality Enhancement Project (HEQEP), AIF (2nd Round)-Sub-Project CP 2099, UGC, MoE, Government of Bangladesh (Contract no. 28/2012).

References

[1] I. McBean, K. Hourigan, M. Thompson, F. Liu, Prediction of flutter of turbine blades in a transonic annular cascade, ASME Journal of Fluids Engineering 127 (6) (2005) 1053–1058.

[2] A.J. Sanders, Nonsynchronous vibration (NSV) due to a flow-induced aerodynamic instability in a composite fan stator, ASME Journal of Turbomachinery 127 (2) (2005) 412–421.

[3] R. Dénos, V. Michelassi, F. Martelli, G. Panjagua, Investigation of the unsteady rotor aerodynamics in a transonic turbine stage, ASME Journal of Turbomachinery 123 (1) (2001) 81–89.

[4] J.B. McDevitt, L.L. Levy, G.S. Deiwert, Transonic flow about a thick circular-arc airfoil, AIAA Journal 14 (5) (1976) 603–613.

[5] L.L. Levy, Experimental and computational steady and unsteady transonic flows about a thick airfoil, AIAA Journal 16 (6) (1978) 564–572.

[6] H. Tijdeman, Investigations of the transonic flow around oscillating airfoils, Ph.D. Dissertation, Faculty of Aerospace Engineering, Delf Univ. of Technology, The Netherlands, 1977.

[7] K. Yamamoto, Y. Tanida, Self-excited oscillation of transonic flow around an airfoil in two-dimensional channels, ASME Journal of Turbomachinery 112 (2) (1990) 723–731.

[8] B.H.K. Lee, Oscillatory shock motion caused by transonic shock boundary-layer interaction, AIAA Journal 28 (5) (1990) 942–944.

[9] A. Alshabu, H. Olivier, I. Klioutchnikov, Investigation of upstream moving pressure waves on a supercritical airfoil, Aerospace Science and Technology 10 (4) (2006) 465–473.

[10] S. Raghunathan, M.A. Gillan, R.X. Cooper, R.D. Mitchell, J.S. Cole, Shock oscillations on biconvex aerofoils, Aerospace Science and Technology 3 (1) (1999) 1–9.

[11] B.H.K. Lee, Self-sustained shock oscillations on airfoils at transonic speeds, Progress in Aerospace Sciences 37 (1) (2001) 147–196.

[12] J. Xiong, S.T. Nezhad, F. Liu, Computation of self-excited unsteady transonic flow of an airfoil in a channel using URANS and DES, AIAA Paper 2010-5109, 2010.

[13] L.W. Chen, C.Y. Xu, X.Y. Lu, Numerical investigation of the compressible flow past an aerofoil, Journal of Fluid Mechanics 643 (2010) 97–126.

[14] A.B.M.T. Hasan, S. Matsuo, T. Setoguchi, A.K.M.S. Islam, Effects of condensing moist air on shock induced oscillation around an airfoil in transonic internal flows, International Journal of Mechanical Sciences 54 (2012) 249–259.

[15] F.R. Menter, Two-equation eddy-viscosity models for engineering applications, AIAA Journal 32 (8) (1994) 1598–1605.